Science of the Total Environment 677 (2019) 502–510

Contents lists available at ScienceDirect

Science of the Total Environment

journal homepage: www.elsevier.com/locate/scitotenv

Insights into thermodynamic mechanisms driving bisphenol A (BPA) binding to extracellular polymeric substances (EPS) of activated sludge

Zi-run Yan [a], Yu-ying Zhu [a], Hui-shan Meng [a], Si-yuan Wang [a], Li-hong Gan [a], Xiu-yan Li [a], Juan Xu [a,b,*], Wei Zhang [c]

[a] Shanghai Key Lab for Urban Ecological Processes and Eco-Restoration, School of Ecological and Environmental Sciences, East China Normal University, Shanghai 200241, China
[b] Institute of Eco-Chongming, East China Normal University, Shanghai 200241, China
[c] State Key Laboratory of Microbial Metabolism, School of Life Sciences and Biotechnology, Shanghai Jiao Tong University, Shanghai 200240, China

HIGHLIGHTS

- Bisphenol A mainly bind with the proteins components of EPS.
- Random-coiled EPS transforms into condensed cores after binding with bisphenol A.
- Binding of bisphenol A to EPS is primarily driven by hydrophobic association.
- Neutral pH, high ionic strength and high temperature promote the binding process.

GRAPHICAL ABSTRACT

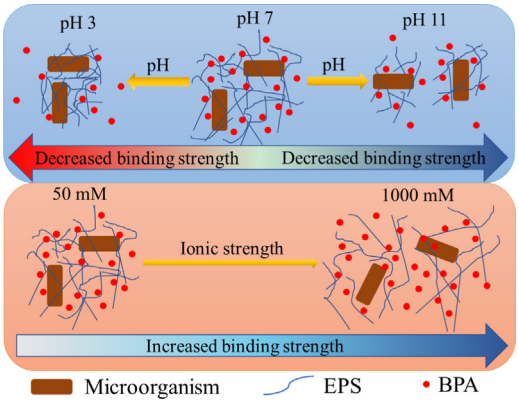

ARTICLE INFO

Article history:
Received 2 March 2019
Received in revised form 24 April 2019
Accepted 27 April 2019
Available online 4 May 2019

Editor: Daniel CW Tsang

Keywords:
Activated sludge
Extracellular polymeric substances (EPS)
Bisphenol A (BPA)
Fluorescence quenching
Isothermal titration calorimetry

ABSTRACT

Bisphenol A (BPA) in wastewater has high risks of causing biological feminization. During the wastewater treatment process, large amounts of BPA are accumulated in activated sludge. However, the mechanisms of BPA interacted with activated sludge are still unclear. Especially, the roles of extracellular polymeric substances (EPS), which are major components of activated sludge, in the removal of BPA have never been concerned. In this study, the binding interactions between sludge EPS and BPA are explored combining fluorescence spectroscopy and dynamic light scattering. The thermodynamic mechanisms driving the binding behavior of BPA to EPS are illustrated by isothermal titration calorimetry. The results indicate that the binding interaction between BPA and EPS is spontaneous. BPA mainly binds with the proteins of EPS by hydrophobic association. The random-coiled structure of EPS transforms into relatively condensed cores after binding with BPA. A neutral pH, high ionic strength, and high temperature promote the binding process, facilitating to stabilize BPA in sludge EPS. This study provides new insights into the roles of sludge EPS in the migration and removal of BPA in activated sludge system.

* Corresponding author at: Shanghai Key Lab for Urban Ecological Processes and Eco-Restoration, School of Ecological and Environmental Sciences, East China Normal University, Shanghai 200241, China.
E-mail address: jxu@des.ecnu.edu.cn (J. Xu).

https://doi.org/10.1016/j.scitotenv.2019.04.413
0048-9697/

1. Introduction

Bisphenol A [2, 2-bis(4-hydroxyphenyl)-propane, BPA] is an endocrine disruptor that significantly induce biological feminization, even at a low-dose exposure of 10^{-7} M (Levy et al., 2004). Due to the wide use of BPA in processing synthetic compounds, the annual production of BPA has reached one million tons globally and keeps increasing at a staggering rate. Therefore, BPA has been extensively detected in waters, soils, and sediments in the environments, thereby seriously threatening public health (Zhao et al., 2014). Generally, BPA from industrial use is discharged into sewage and consequently enters wastewater treatment plants (WWTPs), making WWTPs the largest source of BPA in the natural environment. Currently, BPA is an organic contaminant of great concern in WWTPs in China with concentrations ranging from 140.9 to 3099.6 ng/L (Li et al., 2018).

Over 80% of BPA in wastewater can be removed by conventional activated sludge process in WWTPs. Due to the hydrophobicity of BPA with a high octanol/water partition coefficient (log $K_{ow} = 3.32$), the concentration of BPA in activated sludge is as high as 343 ng/g sludge (Huang et al., 2017). The majority of BPA in wastewater is adsorbed and retained in the sludge (Sun et al., 2017), which is a crucial pathway for BPA removal during activated sludge process. However, deep insights into the mechanisms of BPA accumulation in activated sludge are still lacking.

Previous studies on BPA removal by activated sludge have commonly focused on the removal efficiency and have considered the sludge as an entirety (Ferro Orozco et al., 2013). Recently, subfractions of activated sludge have been identified to make distinct contributions to contaminant removal. As one of the most important components of activated sludge, extracellular polymeric substances (EPS) are complex high-molecular-weight mixture of polymers secreted by microorganisms (Sheng et al., 2010). EPS have strong capability of binding with organic pollutants such as sulfonamides (J. Xu et al., 2013), triclosan (Yan et al., 2019), and phenanthrene (Pan et al., 2010), being ascribed to the existence of hydrophobic regions and functional groups. Considering the characteristics of BPA, there is a strong tendency for BPA to bind with EPS. Since EPS cover the outside surface of activated sludge, the contaminants intercepted in EPS are likely re-released into the surroundings if environmental conditions are changing (Winkler et al., 2007). The existence of EPS would significantly influence the distribution and migration of BPA in activated sludge system. Therefore, it is necessary to explore the binding interactions between BPA and EPS and to identify the crucial factors governing the process.

In this study, the interactions between EPS of activated sludge and BPA are investigated under different environmental conditions, including different pH values, ionic strengths, and temperatures. A combination of fluorescence spectroscopy, gel permeation chromatography (GPC), Fourier transform infrared spectroscopy (FTIR), and dynamic light scattering (DLS) is employed to probe the interactions between EPS and BPA. Isothermal titration calorimetry (ITC) is applied to provide the thermodynamic parameters including entropy change (ΔS), enthalpy change (ΔH), and Gibbs free energy change (ΔG) of the binding interaction. The objective of this study is to ascertain the binding behavior of BPA to sludge EPS under different environmental conditions, as well as to interpret the thermodynamic mechanisms driving the binding process. The results provide new insights into the accumulation of BPA in activated sludge system and highlight the significant roles of EPS in hydrophobic contaminants removal.

2. Materials and methods

2.1. EPS extraction and purification

Activated sludge was collected from the aeration tank of Tianshan WWTP, Shanghai, China. Sludge EPS were extracted by the modified heating method (Xu et al., 2016). This method, developed by Li et al. (Li and Yang, 2007), has been widely used for microbial EPS extraction due to its high extraction efficiency and low cell lysis. The influences of the extraction process on the binding properties of EPS were minimized. Firstly, 70 mL sludge suspension was centrifuged at 8000 rpm for 5 min to dewater. The settled sludge was washed three times with 0.05% NaCl solution. The sludge was then resuspended to the original volume of 70 mL with 0.05% NaCl solution and heated to 60 °C for 30 min in a water bath. The mixture was subsequently centrifuged at 12000 rpm for 15 min. The supernatant comprising EPS was collected and filtrated through a 0.45-μm membrane. Finally, the EPS solution was purified by ultrafiltration with a 3 kDa ultra-membrane to remove the residual NaCl molecules (Amicon Stirred Cell, Millipore Co., USA). The purified EPS solution was then lyophilized (ZX-27, ZhiXin, China) into the powder for the following experiment. The chemical analysis to determine the polysaccharides, proteins, and humic acids in EPS was described in our previous study (Yan et al., 2019). The concentration of EPS was quantified by the total organic carbon (TOC, TOC-Vcpn analyzer, Shimadzu). As shown in Table S1, polysaccharides and proteins are the predominant components of the sludge EPS.

2.2. EPS and BPA binding experiments

EPS powder was dissolved in 50 mM phosphate buffer (PBS) to achieve a concentration of 500 mg/L. Eight tubes were filled with 2 mL of EPS solution and then gradient volumes of BPA solution were added to the tubes. Then 50 mM PBS was added to each tube to maintain a total volume of 10 mL. The final concentrations of BPA were in the range of 0–24 mg/L. Here, the concentration of BPA was magnified to obtain pronounced quenching signals during fluorescence measurements. The high concentrations of BPA and EPS ensured that the ratio of BPA/EPS was similar to that of the wastewater treatment system. Afterward, the solutions were mixed with an oscillator and balanced for 4 h before analysis. The experiments were conducted at the temperatures of 4, 25, and 37 °C. PBS of different pH values and ionic strengths were used to explore the influence of solution conditions on the binding interaction.

2.3. Spectral analysis

Fluorescence spectroscopy, FTIR and UV–Visible (UV–Vis) absorption spectroscopy were used to probe the interactions between EPS and BPA.

Three-dimensional excitation-emission matrix (EEM) fluorescence spectra were measured with a luminescence spectrometer (F-4600, Hitachi Co., Japan) with subsequent scanning emission spectra from 300 to 550 nm at 0.5 nm increments by varying the excitation wavelength from 200 to 400 nm at 5 nm increments. Excitation and emission slits were set at 5 nm and the scanning speed was 1200 nm/min. In order to eliminate second order Raleigh light scattering, a 290 nm emission cutoff filter was applied during measurement. The raw EEM data were corrected with the background, followed by setting the Rayleigh scattering data as zero. Then, the EEM data was processed by parallel factor analysis (PARAFAC) with DOMFluorv1.7 toolbox to obtain the fluorescence intensity score of the EPS components. The details can be found in our previous studies (Sheng et al., 2008; H. Xu et al., 2013).

Synchronous fluorescence spectra were collected for the EPS solution (500 mg/L in 50 mM PBS, pH 7) mixed with gradient concentrations of BPA (0–12 mg/L). Measurements were conducted by synchronously scanning the excitation wavelength from 250 to 400 nm with a constant difference of 60 nm ($\Delta\lambda$) between excitation and emission wavelength. The synchronous fluorescence spectra were processed by two-dimensional correlation spectroscopy (2D-COS) analysis with 2D Shige software (Kwansei-Gakuin University, Japan). The

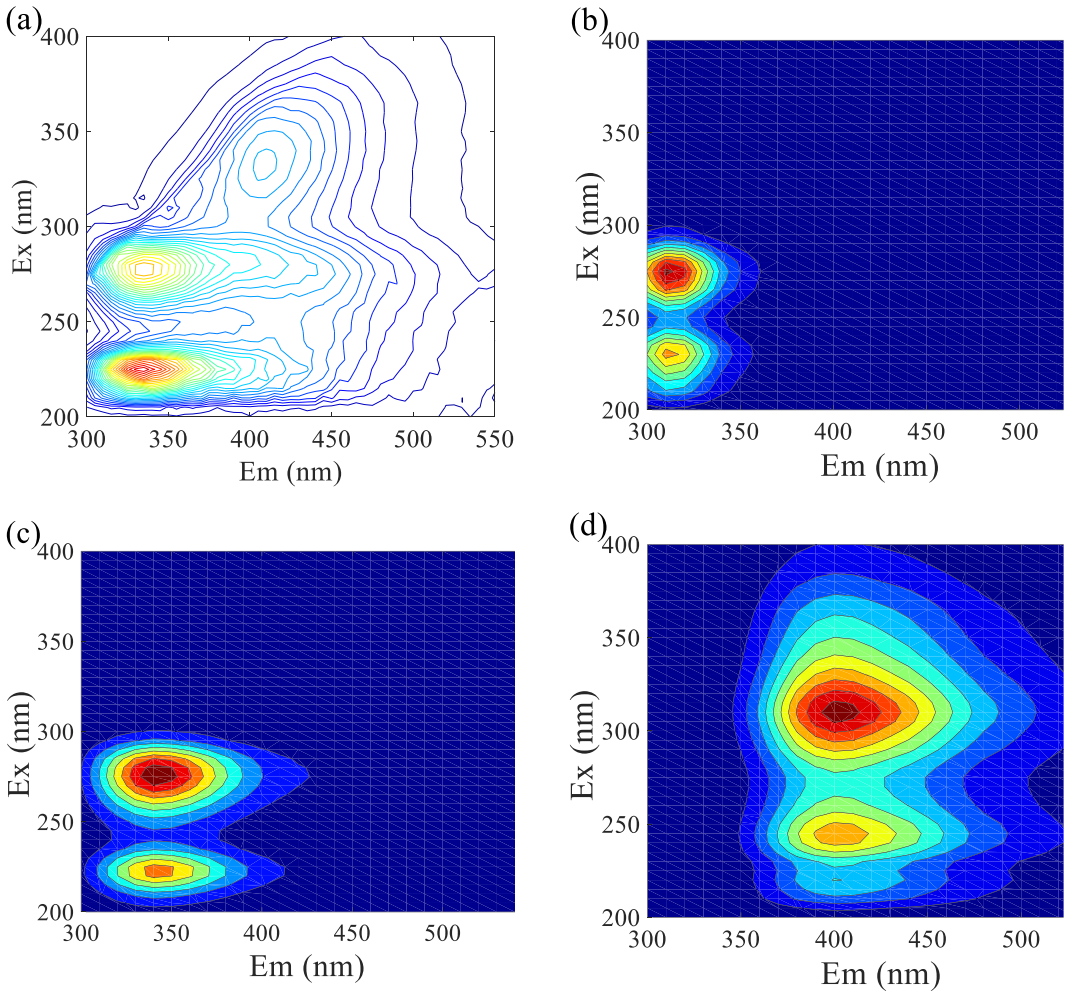

Fig. 1. EEM fluorescence spectra of (a) mixture of EPS and BPA; the individual component of (a) by PARAFAC analysis: (b) BPA, (c) proteins of EPS, (d) humic acids of EPS.

information on the relative directions and sequential orders of the structural variations of EPS binding with BPA was extracted from the auto-peaks and cross-peaks in the synchronous and asynchronous spectra of 2D-COS (Chen et al., 2015; Zhang et al., 2019).

UV–Vis absorption spectra of EPS solution (500 mg/L), BPA solutions (0–15 mg/L), and EPS-BPA complex solutions were obtained using a double beam spectrophotometer (UV-2550, Shimadzu Co., Japan). FTIR was employed to characterize the functional groups of EPS (Nicolet iS5, Thermo Co., USA).

2.4. ITC approach

The thermodynamic mechanisms driving BPA binding to EPS was investigated with an ITC-200 calorimeter (MicroCal Co., USA). BPA and EPS solutions were prepared in a buffer to the final concentrations of 380 mg/L and 5 g/L, respectively. High concentrations of BPA and EPS were utilized to obtain a better resolution of the signals in heat changes since the binding process is independent of BPA concentration (Pelton, 2019). 50 mM Na_2HPO_4-NaOH buffer of two pH values (9.32 and 10.89) were selected to conduct the experiment. All solutions were previously degassed for 15 min under vacuum. There was an initial thermal equilibrium time of 60 s followed by 19 injections. Titrations of BPA into buffer and EPS solution were completed in 2 μL aliquots injected over 4 s during each injection. The experiments were carried out at 25 °C and a stirring rate of 750 rpm.

ITC data treatment was updated based on our previous work (J. Xu et al., 2013), in which the difference in the heat values of two adjacent injections ($Q_i - Q_{i-1}$) was used to represent the heat change (ΔQ_i). Since the reaction and mixing rates were both very fast, the liquid that overflowed from the cell during each injection should also be considered. Assuming that the volume of the overflowed liquid (v) and the same volume of liquid in the cell contributed equally to ΔQ_i, ΔQ_i was expressed by adding a correction term:

$$\Delta Q_i = Q_i - Q_{i-1} + \frac{v}{V_0}\left[\frac{Q_i + Q_{i-1}}{2}\right] \quad (1)$$

where V_0 is the working volume of the cell. The thermodynamic parameters of the binding interaction between EPS and BPA including ΔG, ΔH, and ΔS were acquired by nonlinear fitting of Eq. (1). The details can be found in Supplementary materials.

2.5. Other analyses

Zeta potential and hydrodynamic radius (R_h) of EPS at different pH values and ionic strengths were determined in triplicate by a zeta potential analyzer (NANO ZS3600, Malvern Co., UK) at 25 °C. The molecular weight (MW) distributions of EPS before and after the binding interaction were investigated using a GPC (Waters 1515, Waters Co., USA) equipped with a 7.8 × 300 mm ultra-hydrogel linear column. Each sample was measured in triplicate at 25 °C.

3. Results

3.1. Formation of EPS-BPA complex

EEM fluorescence quenching coupled with PARAFAC analysis was performed to characterize the interactions between EPS and BPA. The EEM fluorescence spectra of the EPS and BPA mixture (Fig. 1a) changed with the addition of BPA; three components were identified, namely BPA (Fig. 1b) (Ex/Em = 275/310 nm), proteins of EPS (Fig. 1c) (Ex/Em = 280/340 nm), and humic acids of EPS (Fig. 1d) (Ex/Em = 310/410 nm) (J. Xu et al., 2013). The spectra of the obtained BPA component were identical to that of the pure BPA solution (Fig. S1), demonstrating the reliability of the PARAFAC analysis. Since no significant quenching was observed for humic acids of EPS, BPA mainly bound with proteins of EPS.

The fluorescence quenching of EPS by BPA was possibly involved in two types of quenching: static quenching due to the formation of a non-fluorescent complex between fluorophore and quencher and dynamic quenching due to the collision between fluorophore and quencher (Chen et al., 2010). UV–Vis spectroscopy was an effective approach to determine the quenching mechanism. If the sum of the individual spectra of EPS (S1) and BPA (S2) was equal to the adsorption spectra of EPS-BPA complex (S3), dynamic quenching was confirmed (S1 + S2 = S3) (J. Xu et al., 2013). However, as displayed in Fig. 2, the differentiated spectra of S1 + S2–S3 varied with the increasing BPA dosage, indicating that static quenching occurred due to the formation of EPS-BPA complex.

2D-COS analysis for the synchronous fluorescence spectra of EPS-BPA complex also confirmed the above-mentioned results. As shown in Fig. 3a, two predominant auto-peaks centered at 265 and 283 nm on the diagonal appeared in the synchronous 2D-COS map, being assigned to BPA and proteins of EPS. The peak at about 340 nm could not be discerned on the map but was deduced from the cross-peaks at (265, 340) and (283, 340). The weak peak at 340 nm, which was attributed to the humic acids of EPS, also indicated that the interaction between humic acids and BPA was less significant. The two cross-peaks in the synchronous 2D-COS map, i.e., (265, 283) and (265, 340), both had negative values, which suggested that the direction of change was the opposite between the substance at 265 nm (BPA) and the substances at 283 and 340 nm (proteins, humic acids) (Chen et al., 2015). Similarly, the positive value at (283, 340) indicated that proteins and humic acids changed in the same direction (i.e., decreased). This finding agreed with the results that the fluorescence of BPA increased whereas the fluorescence of EPS was quenched with the addition of BPA.

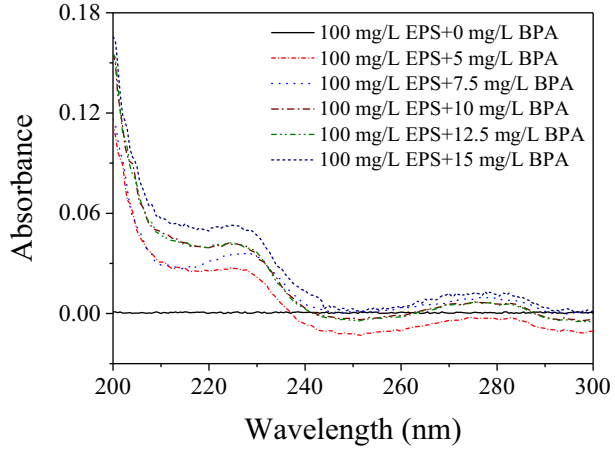

Fig. 2. Differentiated spectra (S1 + S2–S3) between EPS (S1), BPA (S2) and EPS-BPA complex (S3) at various BPA dosages.

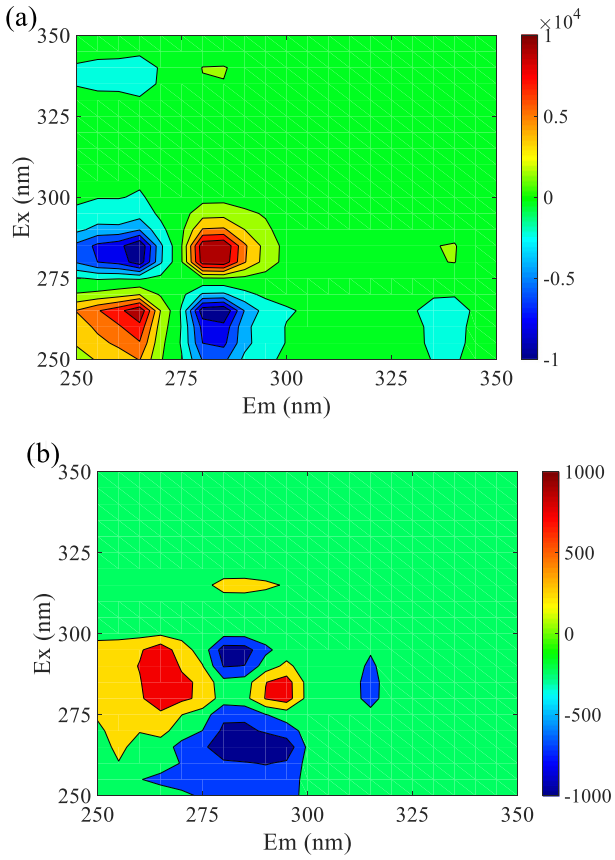

Fig. 3. Synchronous (a) and asynchronous (b) maps generated from the synchronous fluorescence spectra of EPS-BPA mixture by 2D-COS analysis.

Moreover, the asynchronous map (Fig. 3b) provided additional information on the binding sequence between EPS components and BPA. The peak of humic acids shifted to 315 nm and there was a positive cross-peak with proteins at (283, 315). According to Noda's rule (Xu et al., 2018), both positive cross-peaks that were formed by proteins and humic acids in the synchronous and asynchronous maps suggested that proteins bound to BPA prior to humic acids. Therefore, among the two main components in EPS, proteins had stronger affinity and higher priority to bind with BPA than humic acids. The binding of BPA to polysaccharides components of EPS was insignificant due to their instinct hydrophilicity (Tian et al., 2019); however, this was not the focus of this study (J. Xu et al., 2013).

3.2. EPS changes after binding with BPA

The changes in zeta potential of EPS colloids before and after binding with BPA are listed in Table 1. The absolute values of EPS zeta potential decreased with the addition of BPA, indicating a marked reduction in the negative charges of EPS colloids. Since BPA was all in $Bis(OH)_2$ form at pH 7 (Fig. 4), the decreased negativity of EPS zeta potential was mainly caused by configuration changes rather than charge neutralization. The decreased R_h of EPS demonstrated that the random-

Table 1
Variation of zeta potential and configuration for EPS after binding with BPA (pH 7, ionic strength 50 mM, 25 °C).

	Zeta potential (mV)	Hydrodynamic radius (nm)
EPS	−8.43 ± 0.86	159.2 ± 16.6
EPS + 12 mg/L BPA	−3.53 ± 0.81	120.6 ± 9.72
EPS + 24 mg/L BPA	−2.40 ± 1.43	110.0 ± 3.73

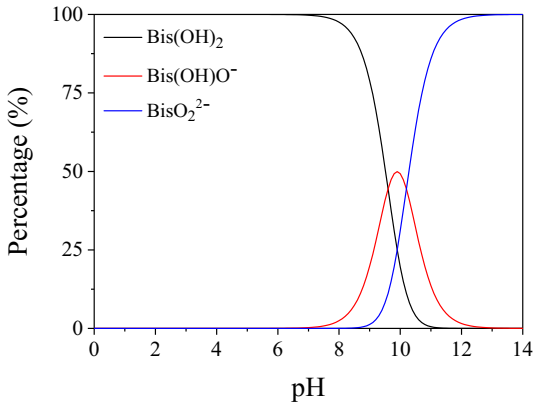

Fig. 4. Distribution of different species of BPA at various pH values.

coiled structure of EPS transformed into relatively condensed cores after binding with BPA (Wang et al., 2012b). This was also consistent with the GPC results in Fig. 5, where a longer retention time indicated a smaller molecular volume (Barth et al., 1998). Both refractive index (RI) and UV signals of EPS shifted slightly to the direction of smaller molecular volume after binding with 12 mg/L BPA. The RI signal reflected EPS colloids, whereas the UV signal was mainly ascribed to the proteins components in EPS. The synchronous variation in RI and UV signals suggested that the decline in the molecular volume of EPS colloids was primarily the result of configuration changes in the proteins. Accordingly, fewer negatively charged groups were exposed due to the dense structure of EPS, leading to a decrease in the absolute value of zeta potential (Table 1).

3.3. Roles of environmental conditions in the binding interaction between EPS and BPA

Since forming EPS-BPA complex, double logarithmic equation was used to calculate the binding constants (K) and binding sites (n) of each component in EPS to BPA (Fu et al., 2016):

$$\log[(F_0 - F)/F] = \log K + n\log[Q]_{BPA} \quad (2)$$

where $[Q]_{BPA}$ is the concentration of BPA, F_0 is the initial fluorescence intensity score from PARAFAC analysis, and F is the fluorescence intensity score after the BPA addition. The parameters of K and n at different pH values are listed in Table 2.

It was found that a neutral condition (pH 7) was more favorable to the binding of BPA to EPS than acid or alkaline conditions. The

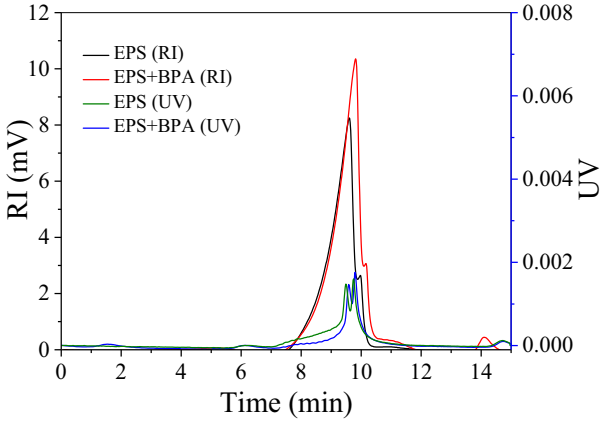

Fig. 5. GPC result of EPS (100 mg/L) before and after binding with BPA (12 mg/L) (pH 7, ionic strength 50 mM, 25 °C).

Table 2
Binding constants (logK) and binding sites (n) of the interactions between EPS and BPA at various pH values (ionic strength 50 mM, 25 °C).

pH	LogK	n
3	3.82 ± 0.015	1.03 ± 0.007
5	4.29 ± 0.030	1.08 ± 0.010
7	4.49 ± 0.110	1.14 ± 0.040
9	3.39 ± 0.015	0.99 ± 0.006
11	3.81 ± 0.040	1.02 ± 0.015

properties of EPS and BPA at different pH values significantly influenced the binding interactions. The zeta potentials and R_h of EPS indicated changes in the surface charge and configuration of EPS colloids at different pH values (Wang et al., 2012b). As shown in Fig. 6a, EPS were positively charged at pH 3 and the value was quite close to the isoelectric point. The negative charges increased gradually on the surface of EPS with increasing pH until a relatively stable zeta potential of −22 mV was reached at pH 9. This was related to the deprotonation of −OH, $-NH_2$, and −COOH (Fig. S2) in EPS with increasing pH (Lin et al., 2016). The R_h reflects the extent to which the particles are drained by the fluid flow. The largest R_h of EPS (212 nm) was observed at pH 5. This was consistent with the results of a previous study, in which the R_h of EPS tended to reach the peak value under weakly acidic conditions. The R_h of EPS was lower under strongly acidic conditions due to the condensed core structure. The R_h of EPS was relatively lower under high alkaline conditions, since large colloids might disintegrate due to the degradation of some EPS components (Wang et al., 2012a). The R_h was higher at pH 11 than at pH 9, implying that EPS molecules stretched slightly at pH 11. Another evidence of the extension of EPS chains was the red-shift of the proteins peak in the EEM spectra at pH 11, as

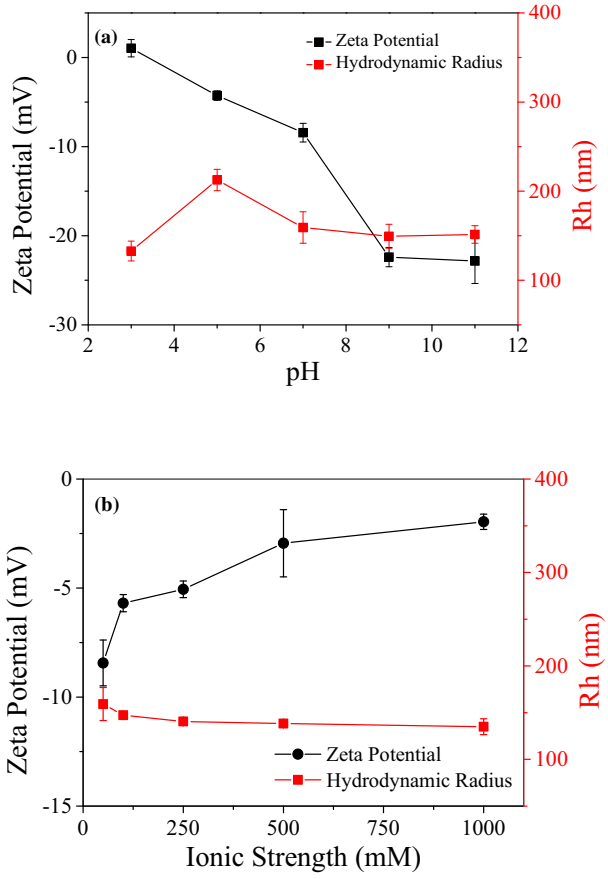

Fig. 6. Zeta potential and hydrodynamic radius of EPS under different pH values (a) and ionic strengths (b).

shown in Fig. S3; this was probably due to the increase in the exposed functional groups (Zhu et al., 2012).

The speciation of BPA evolved with the change in pH values as displayed in Fig. 4. When the pH was lower than 7, BPA existed as $Bis(OH)_2$. H^+ dissociated from −OH of BPA with increasing pH value, whereas BPA existed as $Bis(OH)_2$:$Bis(OH)O^-$:$BisO_2^{2-}$ = 4.5:4.5:1 at pH 9 (Supplementary materials) and mostly as $BisO_2^{2-}$ at pH 11. Since BPA in $Bis(OH)_2$ formed at pH < 7, hydrophobic forces and hydrogen bonds rather than electrostatic effects participated the binding process. EPS colloids gradually aggregated with decreasing pH value, leading to a lower geometrical specific surface area (GSSA) (Wang et al., 2012a). The exposed hydrophobic cavities that BPA was binding with became less available. Therefore, the lower affinity of BPA to EPS under acid conditions was mainly attributed to the configuration changes of EPS. In addition, the protonation portion of amino groups ($-NH_3^+$) in EPS increased with decreasing pH, which disrupted the formation of hydrogen bonds between −OH of BPA and $-NH_2$ of EPS due to the exhaustion of the lone pair of N atoms during protonation (Yang et al., 2008). The reduction in the number of binding sites and the destruction of hydrogen bonds impeded the binding process and resulted in a decrease in the binding constant with dropping pH values.

At pH > 7, the binding process was influenced by the speciation of both EPS and BPA since BPA became ionized in the solvent. The binding constant decreased significantly as the pH increased from 7 to 9. This was mainly attributed to the increasing hydrophilicity of BPA with ionization (Jin et al., 2018). Hydrogen bonds formed between −OH of BPA and −COOH of EPS and disappeared when −OH was ionized to $-O^-$ (Sun et al., 2015). Additionally, electrostatic repulsion was generated between the negatively charged BPA and EPS. The synergistic effects of these three mechanisms significantly inhibited the binding interaction, leading to a lower binding constant at pH 9. However, the binding constant was slightly higher at pH 11 than at pH 9. This was attributed to the larger number of functional groups involved in the binding process because of the molecular stretching of EPS at pH 11.

The increase in the ionic strength induced a continuous decrease in the electronegativity of EPS as shown in Fig. 6b. According to the DLVO theory, the ions compressed the thickness of the electric double layer of EPS colloids, generating a lower absolute value of zeta potential (Tsapikouni and Missirlis, 2007). In addition, the R_h of EPS was slightly decreased as Na^+ entered the EPS colloids to destroy the intra-colloid electrostatic attraction force and hydrogen bonds to deform EPS colloids (Wang et al., 2013).

As shown in Table 3, the binding constant of BPA to EPS increased monotonically with the growth of ionic strength. The reasons are as follows: first, high ionic strength enhanced the hydrophobic interaction between BPA and EPS, which is the fundamental principle of hydrophobic interaction chromatography (Roettger and Ladisch, 1989). Second, as displayed in Fig. 6b, the high ionic strength significantly reduced the electronegativity of EPS colloids, which was beneficial for the binding interaction by weakening the effect of electrostatic repulsion (Li et al., 2007). Third, the high ionic strength destroyed the intra-colloid interactions of EPS to form a looser structure with a larger GSSA and more binding sites (Wang et al., 2013), thereby improving the hydrophobic interaction. Generally, the interactions between BPA and EPS were significantly enhanced at a higher ionic strength.

Table 3
Binding constants (logK) and binding sites (n) of the interactions between EPS and BPA at various ionic strengths (pH 7, 25 °C).

Ionic strength (mM)	LogK	n
50	4.49 ± 0.110	1.14 ± 0.040
100	4.52 ± 0.050	1.08 ± 0.015
250	4.70 ± 0.070	1.12 ± 0.023
500	5.42 ± 0.055	1.28 ± 0.012
1000	5.78 ± 0.091	1.32 ± 0.040

Table 4
Binding constants (logK) and binding sites (n) of the interactions between EPS and BPA at different temperature (pH 7, ionic strength 50 mM).

T (°C)	LogK	n
4	3.70 ± 0.052	0.99 ± 0.019
25	4.49 ± 0.110	1.14 ± 0.040
37	5.21 ± 0.085	1.22 ± 0.015

The influence of the temperature on the interaction between BPA and EPS was also explored (Table 4). It was evident that low temperatures inhibited the binding interaction, which was a result of the endothermic reaction (Isa et al., 2014). The details of the thermodynamic mechanisms of the interaction are described in the following Discussion section.

4. Discussion

Hydrophobic forces, electrostatic effects, and hydrogen bonds were considered to mainly contribute to the binding process between the macromolecular colloids (EPS) and the hydrophobic molecule (BPA). However, the thermodynamic mechanisms driving the binding process evolved under different environmental conditions, which were revealed by ITC approach. pH values of 9 and 11 were selected for the ITC analysis due to the different speciation of BPA. At pH 9, $Bis(OH)_2$ of molecular form and $Bis(OH)(O)^-$ were predominant in solution whereas $Bis(OH)_2$ disappeared at pH 11. The speciation of BPA significantly altered the driving force of the binding interaction between EPS and BPA. As shown in Fig. 7a and c, positive peaks were observed when BPA was titrated into EPS, suggesting endothermic reactions. With the gradual occupation of the binding sites of EPS by BPA, the heat change of the interaction between EPS and BPA attenuated to a stable level. The thermodynamic parameters related to the binding process between EPS and BPA were fitted, as shown in Fig. 7b, d. The binding constants calculated from the ITC approach were logK = 3.19 at pH 9 and logK = 3.48 at pH 11 (Table S2), which agreed well with the results in Table 2. ΔG and ΔS of the interaction were derived as follows:

$$\Delta G = -RT\ln K \quad (3)$$

$$\Delta G = \Delta H - T\Delta S \quad (4)$$

Previous studies on the interactions between BPA and proteinaceous compounds obtained positive values of ΔH and ΔS, such as for human serum albumin (Xie et al., 2010), pepsin (Zhang et al., 2012), and α-Amylase (Hou et al., 2017). A hydrophobic interaction was proposed due to the existence of the hydrophobic pockets formed between tryptophan residues of macromolecular proteins and the aromatic ring of BPA. Thus, a similar mechanism was applicable to the binding process of EPS and BPA since the peak at Ex/Em = 280/340–360 nm in the EEM spectra of EPS could be ascribed to tryptophan residues (Xu et al., 2013b). Therefore, a two-step model was established to describe the interactions between BPA and EPS: the first step was the hydrophobic association of BPA and EPS, which led to the disorder of water molecules (positive ΔH, negative −TΔS); the second step was the formation of a complex involving electrostatic interactions and hydrogen bonds (negative ΔH, positive −TΔS) (Ross and Subramanian, 1981).

Based on the positive ΔH and negative −TΔS (Fig. 8), it is evident that the first step of hydrophobic interaction dominated the binding process. The negative values of ΔG indicated that the binding interaction of BPA to EPS was spontaneous and a stable EPS-BPA complex was formed. The variation of ΔG and its two components ΔH and −TΔS illustrated the specific mechanism of the interaction under different environmental conditions. The greater negative values of ΔG suggested a greater probability of spontaneous interaction. Since the positive ΔH values hindered the binding process, the interaction was

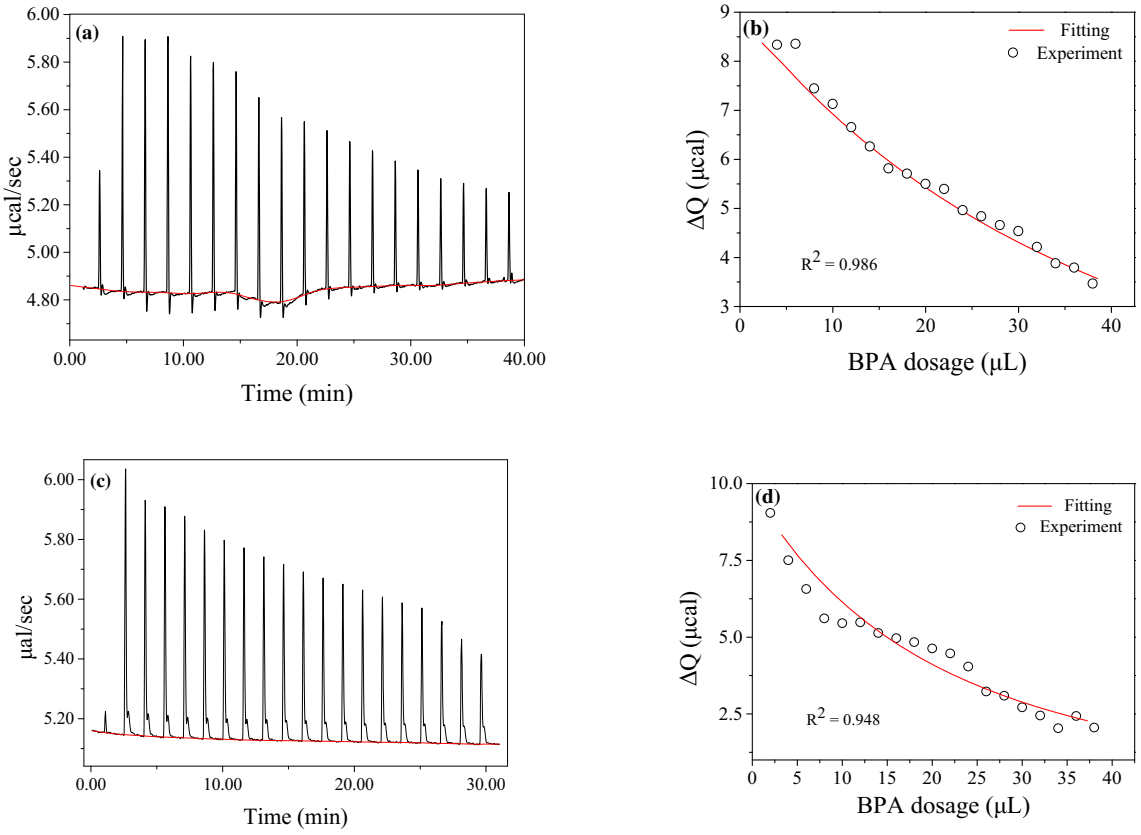

Fig. 7. Thermogram of BPA binding to EPS at (a) pH 9 and (c) pH 11; corresponding nonlinear regression of the heat vs BPA dosage at (b) pH 9 and (d) pH 11.

solely driven by −TΔS. The changes in ΔH and −TΔS were highly correlated with the forces occurring during the interaction. For example, an increase in the pH from 9 to 11 led to the disintegration of hydrogen bonds and augmentation of electrostatic repulsion, which promoted the positive ΔH values. The hydrophobic interaction was enhanced at pH 11 due to molecular stretching of EPS, inducing greater negative values of −TΔS. As a result, the ΔG values remained at a similar level under the two conditions. In spite of similar binding affinities, increase in hydrophobic interaction and electrostatic repulsion, as well as decrease in hydrogen bonds were obtained at pH 11 than at pH 9.

The mechanisms driving the binding of BPA to EPS evolved with changing environmental conditions, as illustrated in Fig. 9. EPS colloids aggregated at low pH values, which resulted in fewer available hydrophobic cavities for BPA to bind with. A high pH caused EPS colloids to swell and disperse, which increased the number of binding sites for BPA. However, the lower hydrophobicity of BPA and greater electrostatic repulsion under alkaline conditions reversed the binding trend, which resulted in lower binding affinity. High ionic strength facilitated to form a loose structure of EPS with more binding sites in addition to enhancing the hydrophobic interaction and weakening the electrostatic repulsion. Thus, the binding affinity increased monotonically with growing ionic strength. The binding process was significantly enhanced by elevating the temperature due to the characteristics of the endothermic reaction. Since a neutral pH, high ionic strength, and high temperature promoted the binding interaction between EPS and BPA, BPA could be effectively stabilized in the sludge system by controlling these crucial factors to strengthen the adsorption process.

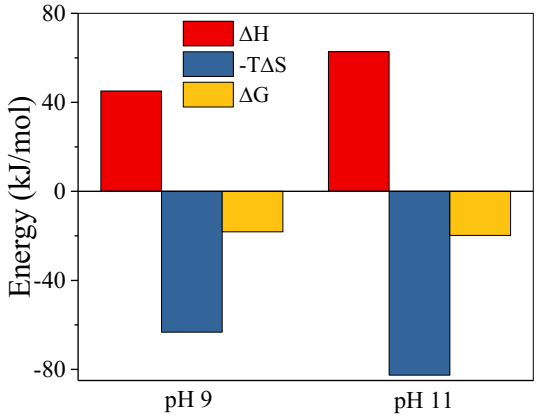

Fig. 8. Evolution of thermodynamic mechanisms driving BPA binding to EPS at different pH values (ionic strength 50 mM, 25 °C).

As the proteins in sludge EPS are the main contributors to the binding interaction with BPA, a higher proportion of proteins in EPS enhanced the binding process. The characteristics of sludge EPS affect the distribution of BPA in activated sludge systems; therefore, sludge from different WWTPs or even from the same WWTP but collected at different times may have different BPA distributions.

5. Conclusions

In this study, the binding behavior of BPA to sludge EPS was demonstrated. BPA mainly bound with the proteins of EPS by hydrophobic association. The random-coiled structure of EPS transformed into a relatively condensed core after binding with BPA. A neutral pH, high ionic strength, and high temperature promoted the binding interaction of sludge EPS to BPA, thus influencing the distribution and migration of BPA in activated sludge systems.

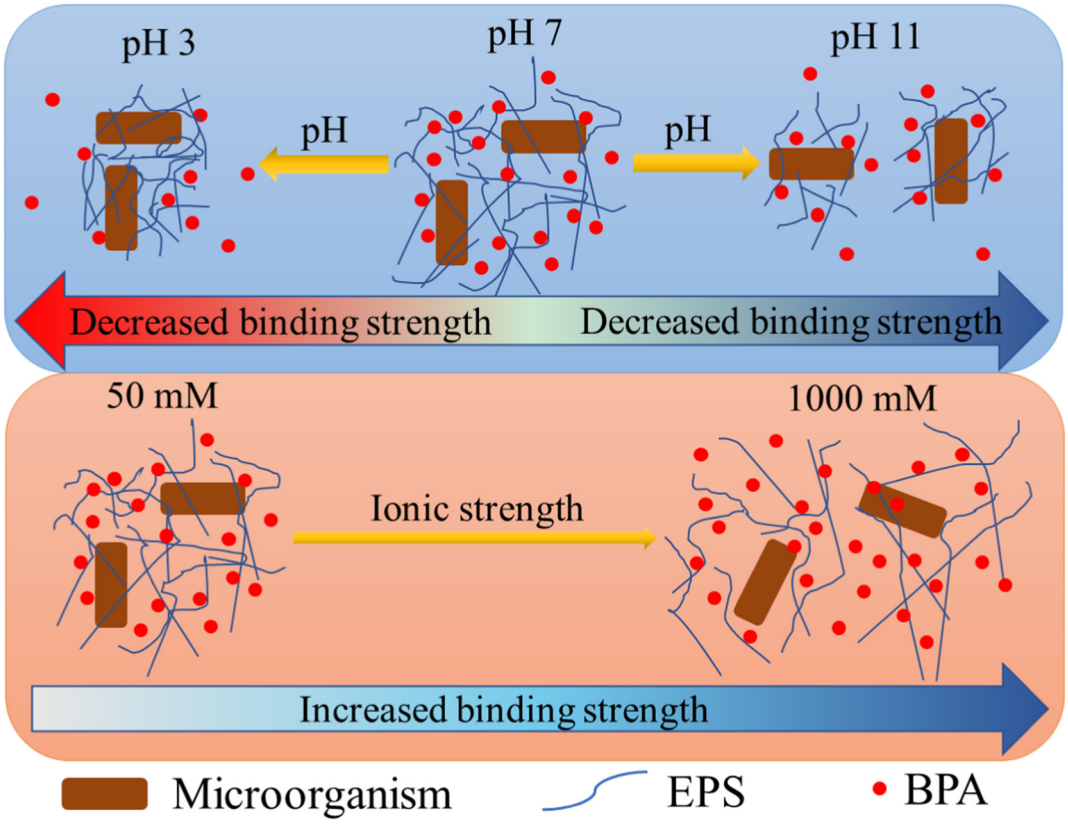

Fig. 9. Schematic illustration for the interactions between EPS and BPA under different environmental conditions.

Acknowledgements

The authors wish to thank National Natural Science Foundation of China (51708224), and the Core Facilities of the School of Life Sciences and Biotechnology in Shanghai Jiao Tong University for the support of this study.

Appendix A. Supplementary data

Supplementary data to this article can be found online at https://doi.org/10.1016/j.scitotenv.2019.04.413.

References

Barth, H.G., Boyes, B.E., Jackson, C., 1998. Size exclusion chromatography and related separation techniques. Anal. Chem. 70, 251–278.
Chen, H., Ahsan, S.S., Santiago-Berrios, M.B., Abruña, H.D., Webb, W.W., 2010. Mechanisms of quenching of alexa fluorophores by natural amino acids. J. Am. Chem. Soc. 132, 7244–7245.
Chen, W., Habibul, N., Liu, X.Y., Sheng, G.P., Yu, H.Q., 2015. FTIR and synchronous fluorescence heterospectral two-dimensional correlation analyses on the binding characteristics of copper onto dissolved organic matter. Environ. Sci. Technol. 49, 2052–2058.
Ferro Orozco, A.M., Lobo, C.C., Contreras, E.M., Zaritzky, N.E., 2013. Biodegradation of bisphenol-A (BPA) in activated sludge batch reactors: analysis of the acclimation process. Int. Biodeterior. Biodegradation 85, 392–399.
Fu, Z., Cui, Y., Cui, F., Zhang, G., 2016. Modeling techniques and fluorescence imaging investigation of the interactions of an anthraquinone derivative with HSA and ctDNA. Spectrochim. Acta A 153, 572–579.
Hou, G., Zhang, R., Hao, X., Liu, C., 2017. An exploration of the effect and interaction mechanism of bisphenol A on waste sludge hydrolysis with multi-spectra, isothermal titration microcalorimetry and molecule docking. J. Hazard. Mater. 333, 32–41.
Huang, R.P., Liu, Z.H., Yuan, S.F., Yin, H., Dang, Z., Wu, P.X., 2017. Worldwide human daily intakes of bisphenol A (BPA) estimated from global urinary concentration data (2000–2016) and its risk analysis. Environ. Poll. 230, 143–152.
Isa, M.H., Ezechi, E.H., Ahmed, Z., Magram, S.F., Kutty, S.R.M., 2014. Boron removal by electrocoagulation and recovery. Water Res. 51, 113–123.
Jin, Q., Zhang, S., Wen, T., Wang, J., Gu, P., Zhao, G., et al., 2018. Simultaneous adsorption and oxidative degradation of Bisphenol A by zero-valent iron/iron carbide nanoparticles encapsulated in N-doped carbon matrix. Environ. Poll. 243, 218–227.
Levy, G., Lutz, I., Kruger, A., Kloas, W., 2004. Bisphenol A induces feminization in Xenopus laevis tadpoles. Environ. Res. 94, 102–111.
Li, X.Y., Yang, S.F., 2007. Influence of loosely bound extracellular polymeric substances (EPS) on the flocculation, sedimentation and dewaterability of activated sludge. Water Res. 41, 1022–1030.
Li, X., Li, Y., Hua, Y., Qiu, A., Yang, C., Cui, S., 2007. Effect of concentration, ionic strength and freeze-drying on the heat-induced aggregation of soy proteins. Food Chem. 104, 1410–1417.
Li, Z., Zheng, T., Li, M., Liu, X., 2018. Organic contaminants in the effluent of Chinese wastewater treatment plants. Environ. Sci. Poll. Res. 25, 26852–26860.
Lin, D., Ma, W., Jin, Z., Wang, Y., Huang, Q., Cai, P., 2016. Interactions of EPS with soil minerals: a combination study by ITC and CLSM. Colloid. Surface. B. 138, 10–16.
Pan, X., Liu, J., Zhang, D., 2010. Binding of phenanthrene to extracellular polymeric substances (EPS) from aerobic activated sludge: a fluorescence study. Colloid. Surface. B. 80, 103–106.
Pelton, A.D., 2019. 2 - thermodynamics fundamentals. In: Pelton, A.D. (Ed.), Phase Diagrams and Thermodynamic Modeling of Solutions. Elsevier, Amsterdam, pp. 9–31.
Roettger, B.F., Ladisch, M.R., 1989. Hydrophobic interaction chromatography. Biotechnol. Adv. 7, 15–29.
Ross, P.D., Subramanian, S., 1981. Thermodynamics of protein association reactions: forces contributing to stability. Biochemistry 20, 3096–3102.
Sheng, G.P., Zhang, M.L., Yu, H.Q., 2008. Characterization of adsorption properties of extracellular polymeric substances (EPS) extracted from sludge. Colloid. Surface. B. 62, 83–90.
Sheng, G.P., Yu, H.Q., Li, X.Y., 2010. Extracellular polymeric substances (EPS) of microbial aggregates in biological wastewater treatment systems: a review. Biotechnol. Adv. 28, 882–894.
Sun, P.C., Liu, Y., Yi, Y.T., Li, H.J., Fan, P., Xia, C.H., 2015. Preliminary enrichment and separation of chlorogenic acid from Helianthus tuberosus L. leaves extract by macroporous resins. Food Chem. 168, 55–62.
Sun, Q., Wang, Y., Li, Y., Ashfaq, M., Dai, L., Xie, X., et al., 2017. Fate and mass balance of bisphenol analogues in wastewater treatment plants in Xiamen City, China. Environm. Poll. 225, 542–549.
Tian, X., Shen, Z., Han, Z., Zhou, Y., 2019. The effect of extracellular polymeric substances on exogenous highly toxic compounds in biological wastewater treatment: an overview. Bioresour. Technol. Rep. 5, 28–42.
Tsapikouni, T.S., Missirlis, Y.F., 2007. pH and ionic strength effect on single fibrinogen molecule adsorption on mica studied with AFM. Colloid. Surface. B. 57, 89–96.
Wang, L.L., Wang, L.F., Ren, X.M., Ye, X.D., Li, W.W., Yuan, S.J., et al., 2012a. pH dependence of structure and surface properties of microbial EPS. Environ. Sci. Technol. 46, 737–744.

Wang, L.L., Wang, L.F., Ye, X.D., Li, W.W., Sheng, G.P., Yu, H.Q., 2012b. Spatial configuration of extracellular polymeric substances of Bacillus megaterium TF10 in aqueous solution. Water Res. 46, 3490–3496.
Wang, L.L., Wang, L.F., Ye, X.D., Yu, H.Q., 2013. Hydration interactions and stability of soluble microbial products in aqueous solutions. Water Res. 47, 5921–5929.
Winkler, G., Fischer, R., Krebs, P., Thompson, A., Cartmell, E., Griffin, P., 2007. Mass flow balances of triclosan in rural wastewater treatment plants and the impact of biomass parameters on the removal. Eng. Life Sci. 7, 42–51.
Xie, X., Wang, X., Xu, X., Sun, H., Chen, X., 2010. Investigation of the interaction between endocrine disruptor bisphenol A and human serum albumin. Chemosphere 80, 1075–1080.
Xu, H., Cai, H., Yu, G., Jiang, H., 2013a. Insights into extracellular polymeric substances of cyanobacterium Microcystis aeruginosa using fractionation procedure and parallel factor analysis. Water Res. 47, 2005–2014.
Xu, J., Sheng, G.P., Ma, Y., Wang, L.F., Yu, H.Q., 2013b. Roles of extracellular polymeric substances (EPS) in the migration and removal of sulfamethazine in activated sludge system. Water Res. 47, 5298–5306.
Xu, J., Yu, H.Q., Li, X.Y., 2016. Probing the contribution of extracellular polymeric substance fractions to activated-sludge bioflocculation using particle image velocimetry in combination with extended DLVO analysis. Chem. Eng. J. 303, 627–635.
Xu, H., Yan, M., Li, W., Jiang, H., Guo, L., 2018. Dissolved organic matter binding with Pb(II) as characterized by differential spectra and 2D UV–FTIR heterospectral correlation analysis. Water Res. 144, 435–443.
Yan, Z.R., Meng, H.S., Yang, X.Y., Zhu, Y.Y., Li, X.Y., Xu, J., et al., 2019. Insights into the interactions between triclosan (TCS) and extracellular polymeric substance (EPS) of activated sludge. J. Environ. Manag. 232, 219–225.
Yang, X., Zhang, X., Liu, Z., Ma, Y., Huang, Y., Chen, Y., 2008. High-efficiency loading and controlled release of doxorubicin hydrochloride on graphene oxide. J. Phys. Chem. C 112, 17554–17558.
Zhang, H., Cao, J., Fei, Z., Wang, Y., 2012. Investigation on the interaction behavior between bisphenol A and pepsin by spectral and docking studies. J. Mol. Struct. 1021, 34–39.
Zhang, X., Yang, C.W., Li, J., Yuan, L., Sheng, G.P., 2019. Spectroscopic insights into photochemical transformation of effluent organic matter from biological wastewater treatment plants. Sci. Total Environ. 649, 1260–1268.
Zhao, J.G., Chen, X.R., Lin, F.K., Yang, N., Huang, H., Zhao, J., 2014. Mechanism of toxicity formation and spatial distribution in activated sludge treating synthetic effluent containing bisphenol A (BPA). Chem. Eng. J. 250, 91–98.
Zhu, L., Qi, H.Y., Lv, M.L., Kong, Y., Yu, Y.W., Xu, X.Y., 2012. Component analysis of extracellular polymeric substances (EPS) during aerobic sludge granulation using FTIR and 3D-EEM technologies. Bioresour. Technol. 124, 455–459.